applied sciences

MDPI

Article

A Hybrid Model for Freight Train Air Brake Condition Monitoring

Alessandro Galimberti, Federico Zanelli and Gisella Tomasini *

Department of Mechanical Engineering, Politecnico di Milano, 20156 Milano, Italy; alessandro.galimberti@polimi.it (A.G.); federico.zanelli@polimi.it (F.Z.)
* Correspondence: gisella.tomasini@polimi.it

Abstract: The Digital Freight Train is expected to revolutionise the rail freight industry. A critical aspect of this transformation is real-time condition monitoring of air brake systems, which are among the leading causes of train malfunctions. To achieve this goal, advanced algorithms for air brake modelling are required. This paper introduces a computationally efficient air brake model tailored for real-time diagnostic applications. A hybrid approach, integrating both empirical data and simplified fluid-dynamic equations, has been adopted. Compared to other air brake models found in the literature, the innovative contributions of the presented model are the reduction of the number of required parameters and the estimation of the brake cylinder pressure directly from the main brake pipe pressure using a feed-forward approach. Moreover, a new approach in the evaluation of the first braking phase and the brake cylinder pressure build-up as the saturation of the brake mode is presented. The model input includes the main brake pipe pressure, the weighing valve pressure, and the brake mode, and the output includes the pressure at the brake cylinder. The air brake model has been validated using data from a previous experimental campaign. The model's accuracy in replicating the air brake system mechanism makes it well-suited for future development of model-based algorithms designed for air brake fault detection.

Keywords: air brake system; hybrid model; brake cylinder; condition monitoring; freight train

Citation: Galimberti, A.; Zanelli, F.; Tomasini, G. A Hybrid Model for Freight Train Air Brake Condition Monitoring. *Appl. Sci.* **2024**, *14*, 11770. https://doi.org/10.3390/app142411770

Academic Editor: Wei Huang

Received: 6 November 2024
Revised: 13 December 2024
Accepted: 15 December 2024
Published: 17 December 2024

1. Introduction

European freight rail transportation is undergoing a transformative shift towards digitalisation, driven by the need for greater safety, reliability and operational efficiency [1,2]. The TRANS4M-R, for example, is a significant European initiative aimed at making rail freight the backbone of a low-emission and resilient transportation network [3,4]. The digitalisation of freight train operations can be achieved by integrating advanced sensor technologies for collecting critical operational data, Condition Monitoring (CM) systems for enabling the detection of potential faults or anomalies [5,6], and Condition-based Maintenance (CBM) systems for optimising maintenance and scheduling interventions. The implementation of real-time onboard monitoring systems has been extensively reviewed in the literature [7–9], focusing on wireless sensor networks and energy-efficient monitoring solutions [10–12] due to the absence of power availability onboard freight trains. Moreover, using models and diagnostics algorithms, it is possible to identify malfunctions in the system and communicate them to a remote-control unit [13,14]. This approach has a huge impact on improving the safety of the convoy, scheduling timely inspections and reducing the cost of maintenance and the number of wagons taken out during service.

The air brake, in particular, is one of the most important and complex systems in railway vehicles. Moreover, compared to the other subsystems of the convoy, the air brake is one of the major components subjected to malfunctions: of the 500 freight rail derailments that occur in Europe each year, approximately 10% are caused by issues related to brake failure [15]. The main causes of railway brake system failure include mechanical

issues and malfunctions, operational mistakes and insufficient maintenance procedures [16]. Moreover, due to its complexity and high compactness, it is often difficult to make a precise diagnosis and identify the malfunction's root causes.

The brake system malfunction is one of the main causes of railway accidents and can have serious repercussions, including service interruptions, derailments, and even fatalities. An example can be found in the runway and derailments of wagons at Ashbury in 2010 [17]. It has been found that the immediate cause of the derailment of five loaded wagons was that the handbrakes were defective due to the wrong adjustment of the handbrake force-limiting bolts. This case illustrates how mechanical failures, coupled with insufficient maintenance protocols, can play a crucial role in triggering catastrophic accidents. A summary report and database of derailment incidents are reported in [18]. It is shown that a key derailment cause in France includes brakes not properly checked or tested, while Great Britain has a higher percentage of derailments as a result of brake failure, the majority of which due to handbrake left applied to wagons when moving on the mainline. An analysis of the causes of failures in the brake equipment of the rolling stock of the railway of Uzbekistan is presented in [19]: it is shown that the main reasons for the withdrawal from the operation of brake pads include air leakage in the distributor and violation of the integrity of the brake pipe due to low tightness of the threaded connection.

An efficient model of the air brake system can be used for malfunction detection during normal service but can also be employed to enhance monitoring effectiveness and minimise necessary resource investments during brake inspections. Current brake inspection procedures require technical operators who manually check the health status of the components within the system: these procedures are time-consuming, wasteful of human power, costly, and not suitable for detecting certain types of failure [20]. Often, inspectors are employed to walk or drive the length of a stationary train, looking for these faults and checking the application to the wheel of the individual brake blocks by visual inspection. In [21], a solution for automatising the brake test relying on pressure sensors is presented. It is shown that the introduction of the brake test system, along with the required automation, is anticipated to reduce the manual effort of the brake test, saving hours of work costs.

The model implemented in this paper is part of a bigger research aiming at developing wireless, modular, and integrated onboard monitoring systems for freight train air brake systems. To optimise the algorithms for the detection of failures, the model should be characterised by low computation cost (for real-time diagnostics) and good accuracy (for recognising multiple brake malfunctions). As described in [22], models for air brake pneumatic components are classified into three main categories: fluid dynamics models, empirical models and fluid-empirical dynamics models.

Fluid dynamics models describe the air brake system components relying on fluid dynamics theories. Those models can describe the dynamic behaviour of the brake systems but are slower in computational speed and are more complicated to develop, and a purely mathematical approach can overlook the mechanical behaviour and physical working principle of the air brake system. In [23], an approach for simulating air brake systems of long freight trains based on fluid dynamics theory is proposed. The fine spatial mesh along the length of the main brake pipe and the explicit time-stepping methods to stabilise the solution and manage the pressure wave oscillations accurately are important features for developing high-resolution and precise simulations. However, these methods introduce a significant computational overhead: the simulation process takes an average of some minutes to simulate just a few seconds of braking response, rendering it impractical for real-time application. In [24], a total number of 41 parameters were used to develop a detailed fluid dynamics air brake model, which includes subsystem models for pipes, wagons and locomotive brake valves. The average simulation time for the conventional sequential computing scheme is about 6.7 times slower than in real-time, making this model impractical for onboard diagnostics. Real-time simulations are achieved by parallel computing using eight computer cores: this hardware configuration will re-

quire high-performance computing (HPC) capabilities that are unsuitable for freight train onboard applications.

Empirical models are simple and faster in computational speeds but have lower generalisation due to the high dependency on the experimental data used to develop the model. [25] shows the development of a strategy for the calculation of the air brake forces of European freight trains using an empirical exponential function. The model does not require the detailed simulation of the fluid dynamics in the brake pipe nor the precise knowledge of the main parameters of the braking system mounted on each vehicle. The model described in [26] uses a two-dimensional look-up table to determine the cylinder pressure in freight train air brakes. Cylinder pressures of the first and last vehicle of the convoy are used as reference pressures and identified from measured data, while the corresponding value of intermediate convoys is then interpolated by indexing the position of the vehicle. These two approaches are unsuitable for real-time diagnostic purposes since they lack the granularity to accurately simulate internal brake pressure variations in real-time contexts and show low generalizability since they are less adaptable to varying operational conditions.

In the end, in [27], an example of a fluid-empirical dynamics model based on a lumped parameter scheme is presented. The model is adopted to represent the main brake pipe with the possibility of venting the pipe from different positions. Pressure build-up in brake cylinders is determined by the dynamics of pressure drop in the main brake pipe and by the crossing of pressure thresholds. This model is particularly suitable for onboard real-time diagnostics of railway brake systems due to its balance of accuracy, computational efficiency and generalisability. The model is highly accurate in simulating the dynamics of the main brake pipe, but it has significant limitations in modelling the dynamics of the brake system itself since critical components such as the weighing valve, the kink valve and the relay valve are not considered. Furthermore, the model does not account for the release phase, which is essential for identifying specific failures, such as improper brake detachment from the wheel, which can lead to wear of the brake pad, material build-up and overheating. Additionally, the model is restricted to simulating emergency braking and does not include service braking, which is the predominant braking action during nominal operations, where the brake cylinder response is more influenced by the gradual depression of the main brake pipe rather than the brake mode.

Simulation experience indicates that a fluid dynamic air brake model can be 100 times slower than its empirical counterpart, that is, in general, faster than real-time [22]. Therefore, a fluid-empirical dynamic model can be used to achieve real-time monitoring, and this approach has been selected for the brake system modelled in this paper.

Compared to fluid dynamics models ([23,24]), the model presented in this paper is characterised by a total of 18 parameters. Moreover, thanks to the feed-forward approach in estimating the brake cylinder pressure from the main brake pipe pressure, bypassing the need for feedback from the auxiliary reservoir and the evaluation of the brake cylinder build-up pressure from the brake mode saturation in the relay valve, the computational cost is significantly reduced. Compared to the fluid-empirical dynamics model presented in [27], the model presented in this paper contains a new approach for the simulation of the first braking phase. It is not based on threshold settings but on the correlation between the brake cylinder pressure and the distributor pressure variation derived by the activation of the accelerated chambers. While most of the models found in the literature are focused on replicating the brake cylinder steady state condition, the higher accuracy reached in simulating the first braking phase allows for improving the ability of the diagnostic model to recognise malfunctions that are usually very difficult to detect (i.e., push-rod out of adjustment, higher stroke of the brake cylinder piston, variation of the stiffness of the brake cylinder spring and manual brake activation during train moving condition). Moreover, compared to [27], the simulation of different brake components, such as the weighing valve, the kink valve, the relay valve and the brake release valve, enables an increase in the efficiency of the model. With the main brake pipe pressure as an input parameter,

the air brake model can also simulate service braking action rather than focusing only on emergency braking, as in [27]. As shown in the Results Section, the model's accuracy in replicating the air brake system mechanism makes it well-suited for future evaluations of model-based algorithms designed for air brake fault detection.

This paper presents the description of a hybrid air brake model that uses both simplified fluid-dynamic models and empirical models to estimate the transfer function between the main brake pipe pressure and the brake cylinder pressure. In Section 2, the air brake model is presented, focusing the attention on the description of the T3000e wagon brake system configuration used as a reference for modelling and validating the air brake model, the algorithms for pre-processing the input variables and the model of the air brake main components. In Section 3, the main parameters used for modelling the air brake system are presented, and the model validation through experimental dataset comparison from the campaign reported in [28] is shown. In Section 4, results, conclusion and possible further developments are reported.

2. Materials and Methods

The air brake model presented in this paper is part of a collaborative research initiative with Mercitalia Intermodal (Milan, Italy) aimed at setting up real-time diagnostic algorithms of freight train braking systems to be implemented into a wireless onboard monitoring system [29,30]. The graphical abstract in Figure 1 outlines the methodological approach adopted to achieve this diagnostic target. A key aspect of the approach is the implementation of an air brake model using Matlab R2021b software [31] to accurately estimate the brake cylinder pressure. Any discrepancies between the estimated and experimentally monitored brake cylinder pressure can serve as indicators of potential faults in the air brake components.

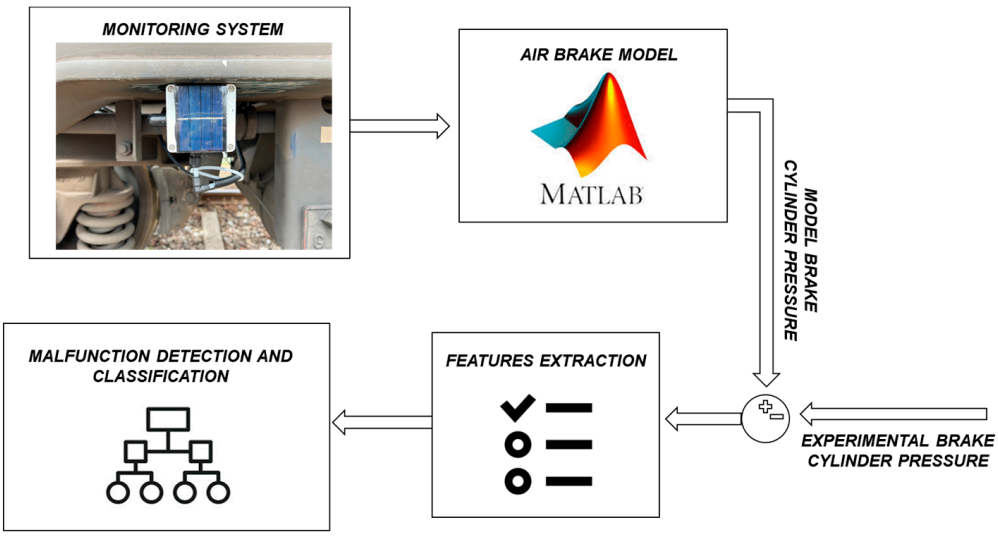

Figure 1. Graphical abstract of the methodological approach adopted.

2.1. T3000e Wagon Air Brake Plant

The air brake model has been developed and validated on the basis of the experimental dataset coming from the brake monitoring system of the T3000e wagon during the campaign described in [28]. The detailed schematisation of the T3000e wagon air brake plant is shown in Figure 2.

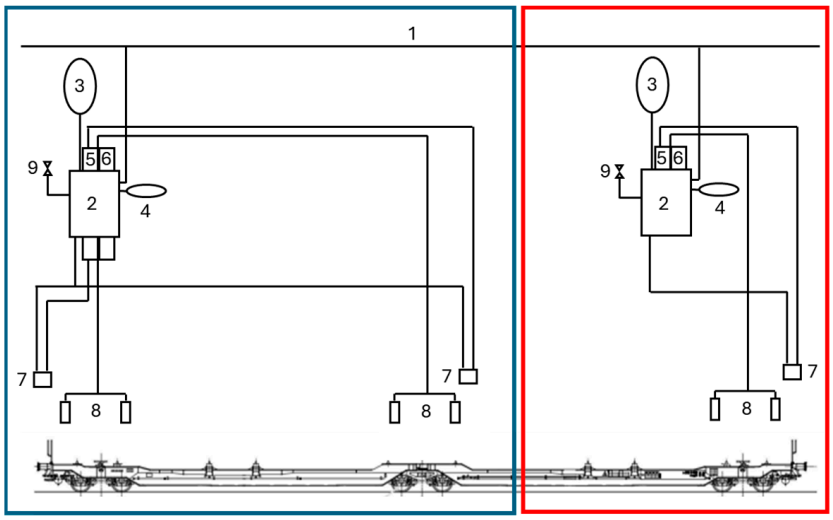

Components	Description
1	Main brake pipe
2	Distributor
3	Auxiliary reservoir
4	Control reservoir
5	Kink valve
6	Limiting valve
7	Weighing valve
8	Brake cylinder
9	Release valve

Figure 2. T3000e wagon air brake plant scheme.

The double pocket wagon is equipped with a pneumatic brake system with three load-proportional braking devices, each of them acting upon the composite brake blocks. The braking device in the central bogie consists of one weighing valve and one brake cylinder with an external slack adjuster, while the braking devices in the lateral bogies consist of one weighing valve and two brake cylinders equipped with internal slack adjusters.

Each load-proportional device is as follows:

- Controlled by a distributor, and its braking performance is determined independently for each bogie;
- Installed in the chassis frame and consists also of one relay valve and one limiting valve with universal test points for brake testing

In the blue box of Figure 2, the braking action in the lateral and central bogie braking device is controlled by a bigger and unique distributor and requires an auxiliary reservoir volume of 125 L, while in the red box, the braking action of the lateral bogie braking device is controlled by a smaller distributor and requires an auxiliary reservoir volume of 75 L.

The distributors are equipped with ON/OFF and freight-passenger (G | P) changeover devices. The double pocket wagon is equipped with a continuous main brake pipe with isolation cocks and brake–hose couplings. The brake force on each bogie is adjusted to load through the weighing valve [32].

2.2. Model Flow Chart and Data Pre-Processing

In Figure 3, a schematic overview of the air brake system model flow chart is shown. In the acquisition stage, the monitoring system (of the same type as the one described in [28]) gathers experimental data from three key points: the main brake pipe, the weighing valve and the brake cylinder. The main brake pipe pressure is then pre-processed to identify the time intervals for braking, holding and releasing phases. These phase durations, along with the main brake pipe pressure, weighing valve pressure and the model parameters, serve as inputs to the air brake model, which outputs the expected brake cylinder pressure. The model validation is then performed by comparing the experimental and the model brake cylinder pressure. Any deviation between the modelled and experimental brake cylinder pressures can indicate potential malfunctions within the system, as illustrated in Figure 1.

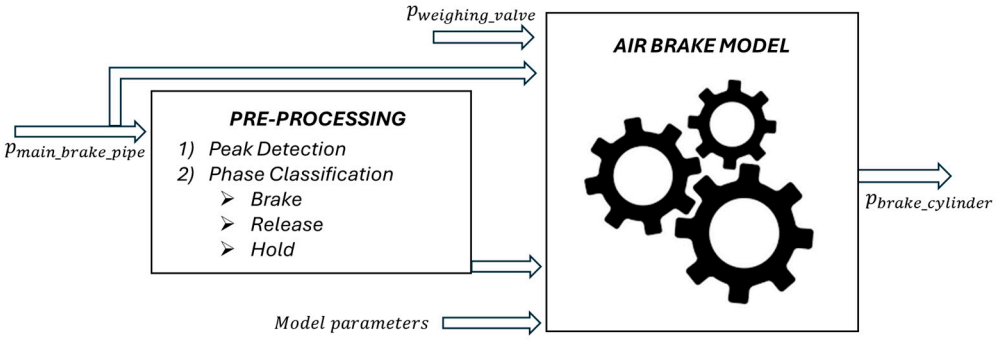

Figure 3. Air brake system model flow chart overview.

The brake cylinder response is influenced by several factors: the main brake pipe pressure, which enables the simulation of both service and emergency braking; the weighing valve pressure, which allows for the simulation of different loading conditions; the model parameters, which allow testing different brake system configurations and brake modes (freight or passenger).

Before the main brake pipe pressure is introduced as input in the model, it undergoes a two-step pre-processing phase: peak detection and phase classification. During peak detection, the time history of the main brake pipe pressure, recorded during acquisition, is divided into distinct braking actions, as shown in Figure 4b. The time history of the main brake pipe pressure is first filtered using a moving average filter to reduce noise. Then, the time derivative of the filtered signal is calculated. The minima peaks in the derivative correspond to the start of the brake action, indicating moments of instantaneous pressure reduction in the main brake pipe, as shown in Figure 4a. The initial pressure value of the main brake pipe at the start of each braking action is then determined, which is crucial because this value is held constant in the control reservoir and regulates the pressure transmitted to the distributor.

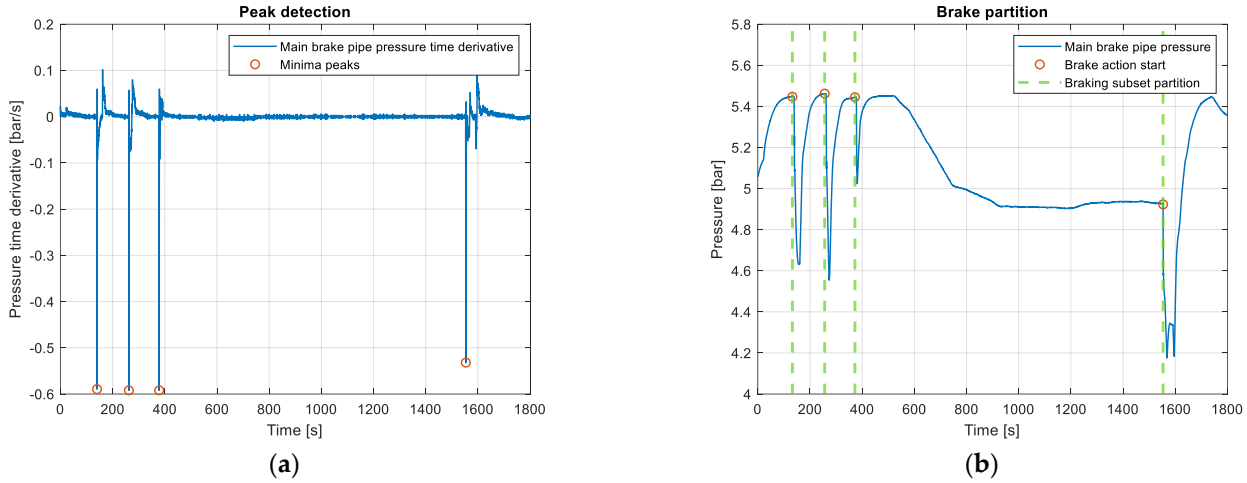

Figure 4. Time histories of (**a**) the main brake pipe peak detection algorithm and (**b**) the main brake pipe partition.

A phase classification algorithm is then used to identify three main braking conditions: braking, releasing and holding. The braking phase begins with a decrease in the main brake pipe pressure, triggering the distributor to feed air into the brake cylinder, increasing its pressure until stabilisation. The holding phase follows, where both the main brake pipe and brake cylinder pressures remain constant, maintaining the braking force. Finally, the releasing phase starts when the main brake pipe pressure rises, signalling the distributor to vent the brake cylinder, reducing its pressure and fully releasing the brakes. The algorithm

is based on the distributor pressure, calculated as the depression between the main brake pipe pressure (Figure 5a) and the control reservoir pressure: this signal is passed through a moving average filter to cut off the fast dynamics related to the accelerated chambers activation (Figure 5b, p_{filter}) and then a first-order differential function is applied (Figure 5c, $\dot{p}_{filter}$). The braking condition starts when $\dot{p}_{filter}$ is higher than 0.005 bar/s, while the releasing is the condition where $\dot{p}_{filter}$ is lower than −0.005 bar/s, and the holding is the intermediate condition, as shown in Figure 5d.

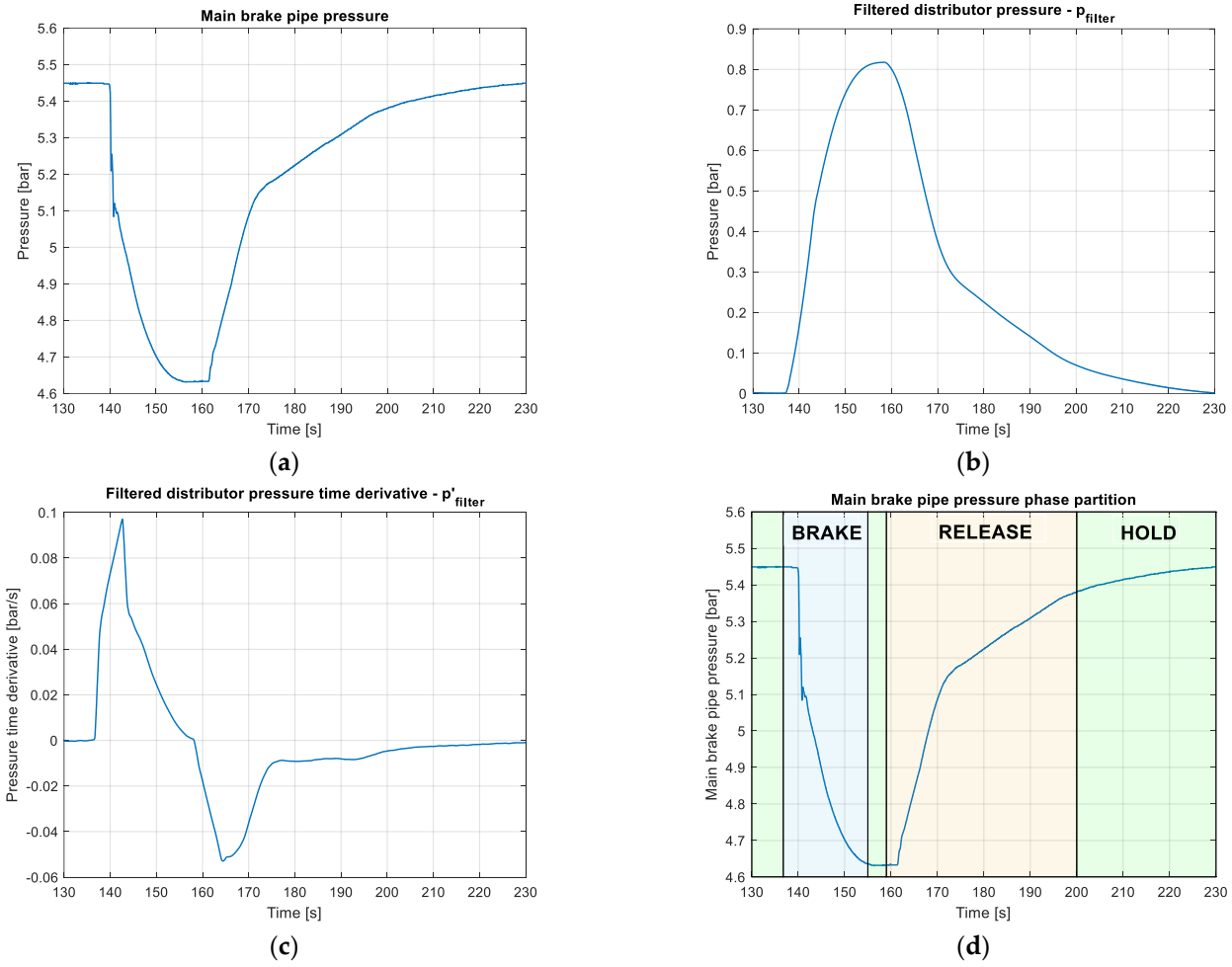

Figure 5. Time histories of (**a**) main brake pipe pressure, (**b**) filtered distributor pressure, (**c**) Filtered distributor pressure time derivative and (**d**) main brake pipe pressure phase partition and classification.

The information regarding the phase partition and classification is introduced inside the model. A hybrid air brake model using empirical and fluid-dynamic simplified equations is used to evaluate the brake cylinder pressure. A simplified model of the distributor combined with fluid dynamic considerations of the first braking phase and the releasing phase and empirical transfer function for evaluating the command pressure at the relay valve is presented in Section 2.3. Figure 6 presents a simplified scheme of the detailed air brake plant, as shown in Figure 2, with the main components. Each air brake pipe pressure is either controlled or uncontrolled depending on the presence of a valve in the passage between consecutive chambers. The algorithm takes into input the main brake pipe pressure and weighing valve pressure coming from the sensor acquisition, and, according to the implemented transfer function, it provides the output of the brake cylinder pressure.

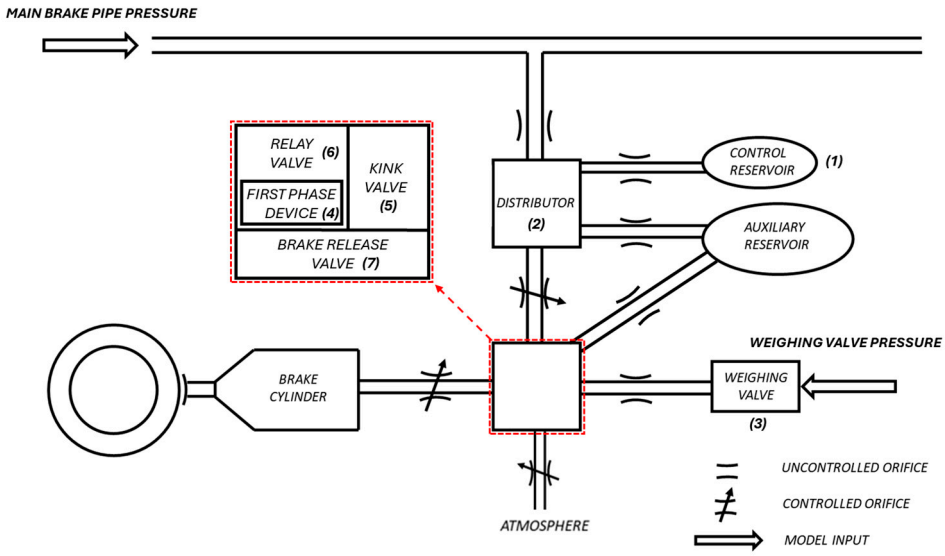

Figure 6. Simplified scheme of the air brake system.

The presence of a load braking action independent on each bogie allows the modelling of a generalised brake system, which can then be tuned to model-specific configurations (i.e., the central or lateral bogie braking system) and the block schematisation of the air brake main components shown in Figure 6, each with their own transfer function enables model generalisation to wagons with different air brake systems (i.e., air brake system lacking a weighing valve or with a different kink valve transfer function).

2.3. Main Components Implemented in the Model

2.3.1. Control Reservoir

The control reservoir (labelled (1) in Figure 6) is modelled as a constant pressure volume through the braking application, and its pressure is used to regulate the distributor pressure. The connection between the main brake pipe and the control reservoir is modelled with a sensitivity valve. For small main brake pipe pressure variations, the valve remains open, and the two pressures will equalise each other. For high main brake pipe pressure variations, the valve will close out, keeping the control reservoir pressure at the main brake pipe starting pressure.

2.3.2. Distributor

The distributor (labelled with (2) in Figure 6) pressure (p_d) is modelled as the depression of the main brake pipe pressure (p_{mbp}) from the control reservoir pressure (p_{cr}), ranging between 0.1 bar and 1.5 bar. The first pressure parameter (identified as Act in Table 1) is related to the distributor activation: for a pressure drop lower than this value, the braking action is not activated, and the distributor valve remains closed with a zero-pressure reference. The activation threshold has been empirically tuned to model the time lag of the brake plant mechanical system, resulting in a braking activation time in the main brake pipe that is different from the activation time in the brake cylinder. With a pressure drop of 1.5 bar (identified as Dmax in Table 1), the brake cylinder develops the maximum braking force, resulting in the distributor pressure saturation. This parameter comes from the UIC 540-0 normative [33]. In Figure 7a, the simplified scheme of the distributor is reported, while in Figure 7b, the free body diagrams of the forces acting on the piston-valve assembly of the distributor are shown.

Table 1. Model brake system parameters.

Component	Parameters	Value	Description	Source
Brake plant	Vmin	0.005 m^3	Brake cylinder minimum volume	T3000e specs
	Vmax	0.01 m^3	Brake cylinder maximum volume	T3000e specs
Distributor	Tchar	24 s	Normative braking time based on G mode activation	UIC Normative
	Act	0.1 bar	Distributor activation pressure	T3000e specs
	Dmax	1.5 bar	Distributor saturation pressure for full-service braking	UIC Normative
Braking phase	Fb	0.4 bar	First phase braking ending pressure at the brake cylinder	T3000e specs
	EQP	0.15 bar	Equivalent spring pressure for relay alimentation valve opening control	T3000e specs
	Pmax	3.6 bar	Maximum braking pressure at the brake cylinder	UIC Normative
Kink valve	K0	0.2 bar	Distributor pressure for kink valve S-mode activation	T3000e specs
	K1	0.7 bar	Distributor pressure for kink valve S-mode de-activation	T3000e specs
	LIM1	1.36 bar	Distributor pressure for kink valve load saturation in the braking phase	T3000e specs
	LIM2	1.2 bar	Distributor pressure for kink valve load saturation in the releasing phase	T3000e specs
Releasing phase	Sact	0.68 bar	Distributor pressure for release activation	T3000e specs
	S1	0.175 bar	Brake cylinder pressure for ending efflux	T3000e specs
	Tin	273.18 K	Ambient temperature	Physical parameter
	R	287.1 J/kgK	Gas constant	Physical parameter
	patm	1 bar	Atmospheric pressure	Physical parameter
	A	0.0000125 m^2	Orifice area for release in G mode	T3000e specs

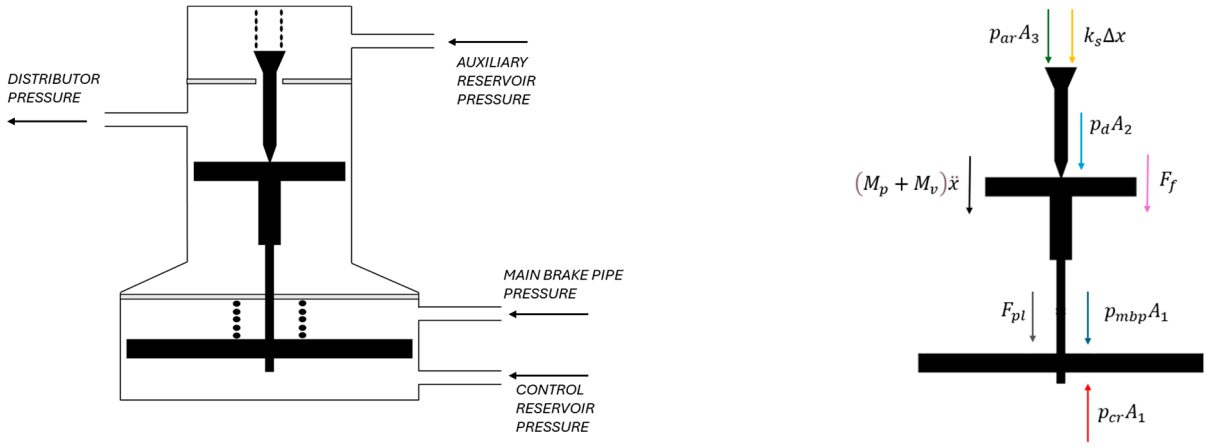

(**a**) (**b**)

Figure 7. Schematic overview of (**a**) the distributor and (**b**) a free body diagram of the forces acting on the piston-valve assembly of the distributor.

The equation of motion of the piston-valve assembly of the distributor is reported in Equation (1).

$$(M_p + M_v)\ddot{x} = (p_{cr} - p_{mbp})A_1 - p_{ar}A_3 - p_dA_2 - k_s\Delta x - F_{pl} - F_f \quad (1)$$

where M_p and M_v are the distributor piston mass and opening valve mass connecting the auxiliary reservoir to the distributor outlet pipe, p_{cr} is the pressure at the control reservoir,

p_{mbp} is the pressure at the main brake pipe, p_{ar} is the pressure at the auxiliary reservoir, p_d is the pressure at the distributor outlet pipe, k_s is the equivalent spring term derived by the equivalent connection in a series of piston and valve springs, A_1 is the piston surface on which the control pressure and the main brake pipe pressure act, A_3 is the valve surface area on which the auxiliary reservoir pressure acts on, A_2 is the piston surface on which the distributor pressure acts, Δx is the spring elongation represented by the piston-valve assembly stroke, F_{pl} is the spring pre-load and F_f is the friction force coming from the mechanical system interconnection.

Starting from Equation (1), it is possible to derive a simplified model of the distributor based on the following considerations. Given the piston masses in the order of 10^1 kg, to have the piston inertial contribution comparable with the pressure forces (in the order of 10^3 N), the acceleration of the piston-valve assembly during braking should be proportional to 10^2 m/s^2. This is not the case for air brake systems for freight train applications, where inertial terms are usually an order of magnitude lower than pressure forces terms. The inertial contribution can, therefore, be neglected. The spring force coming from the piston-valve assembly movement can be considered a constant force, like the spring pre-loading force, due to the limited stroke variation. In this way, since these two terms do not introduce a differential term during the pressure build-up, they can only affect the distributor activation and saturation pressure. Considering the distributor as an ideal mechanical component (i.e., sliding surface well lubricated), the friction forces can be set to zero. Moreover, since the auxiliary reservoir pressure acts on a surface much smaller than the others, its force contribution can be neglected. With these assumptions, it is possible to derive a proportionality law between the distributor pressure and the main brake pipe pressure, as reported in Equation (2).

$$p_d = \left(p_{cr} - p_{mbp}\right)\frac{A_1}{A_2} \tag{2}$$

Considering a 1:1 ratio between the distributor pressure area and the main brake pipe pressure area, it is possible to model the distributor pressure as the depression of the main brake pipe pressure from the control reservoir pressure. This assumption is based on the reasonable consideration that the two areas A_1 and A_2 are comparable.

In Figure 8, a comparison between the main brake pipe pressure coming from the experimental monitoring system and the modelled distributor pressure is shown.

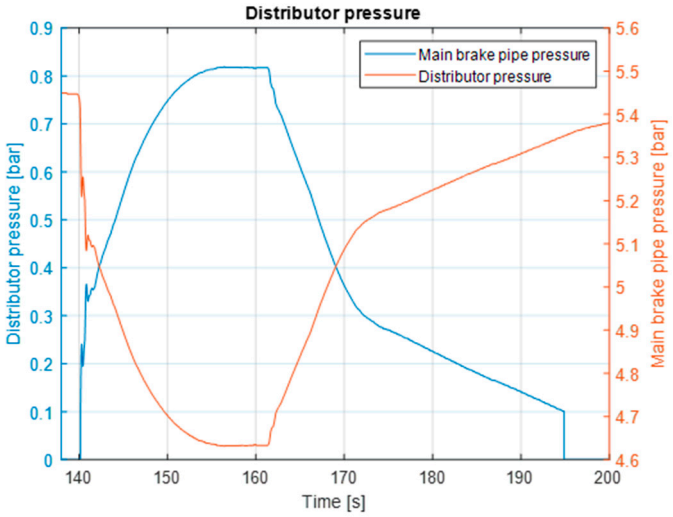

Figure 8. Comparison between the main brake pipe pressure and the distributor pressure.

2.3.3. Weighing Valve

The wagon weighing valve pressure (labelled with (3) in Figure 6) is considered an input parameter in the model. Starting from the full wagon configuration, the weight is distributed on the central and lateral bogie through the transfer loading function reported in Figure 9a. Two different transfer functions have been identified, given that the central bogie is usually more loaded than the lateral bogies. As shown in Figure 9b, the linear weighing valve transfer function is identified. These two transfer functions have been derived from the wagon technical specifications provided by Mercitalia Intermodal.

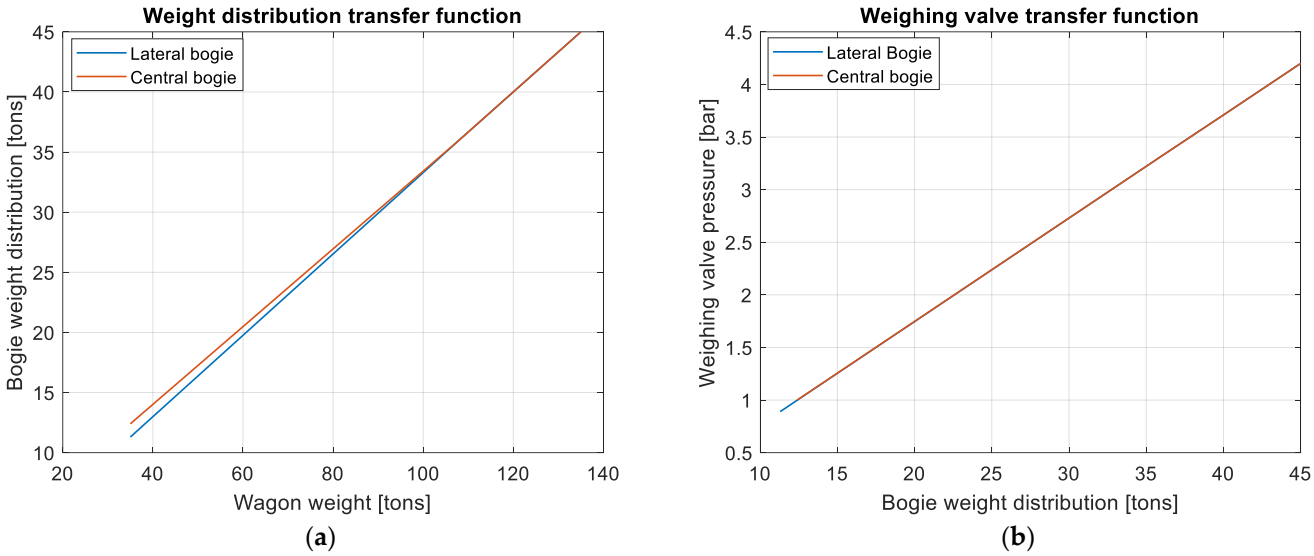

Figure 9. Transfer function of (**a**) wagon weight distribution and (**b**) the weighing valve.

2.3.4. First Phase Device

The first phase device (labelled (4) in Figure 6) is a complex component that can be considered as a feature of the relay valve component. It defines a non-linear correction of the brake cylinder pressure depending on the distributor pressure variation. The first braking phase provides a large opening connection between the auxiliary reservoir and the brake cylinder. This device allows the brake cylinder to be rapidly filled with compressed air and to apply nearly 15% of its maximum force [27], keeping the brake in contact with the wheel. The first braking phase ends when the brake cylinder pressure reaches 0.4 bar (identified as Fb in Table 1).

While in the literature [27] the first braking phase is modelled through threshold settings tuned from the experimental dataset, causing an increase in the number of model parameters to be identified and a loss of air brake model generalisation, in this paper, the first braking phase is modelled by studying the correlation between the brake cylinder response and the distributor pressure variation caused by the activation of the accelerated chambers, representing thus a novel approach. While most of the models found in the literature are focused on replicating the steady-state condition of the brake cylinder pressure, the simulation of the first braking phase allows to improve the ability of the diagnostic model to recognise malfunctions that are usually very difficult to detect (i.e., push-rod out of adjustment, higher stroke of the brake cylinder piston, variation of the stiffness of the brake cylinder spring and manual brake activation during train moving condition). Since the accelerated chambers are small volume reservoirs, the filling by the main brake pipe determines an instantaneous reduction of the main brake pipe pressure followed by a limited pressure increase derived by a flux-out mechanism, as reported in [34]. Since the distributor is modelled as the main brake pipe depression, we can correlate the activation of the first braking phase with the distributor pressure variation. In Figure 10a,b, a schematic overview of the activation and de-activation of the first braking phase is shown.

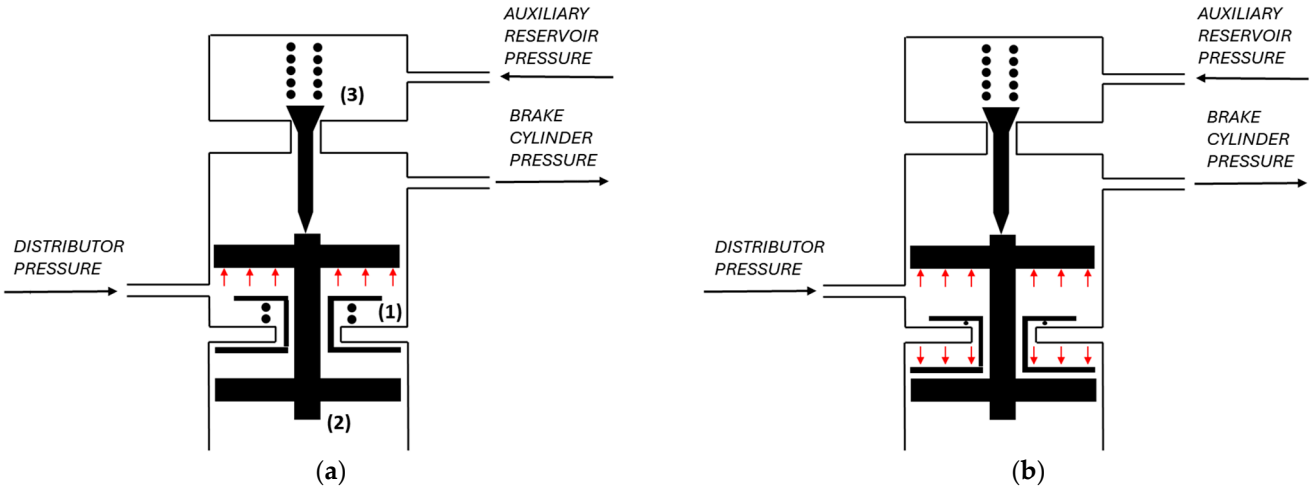

Figure 10. Schematic overview of (**a**) first braking phase activation and (**b**) first braking phase de-activation.

During the first braking phase, the alimentation piston sub-assembly (1) is blocked by the spring compression pre-loading force. If the distributor pressure is not able to overcome the pre-loading condition of the spring, its contribution only affects the upper surface of the alimentation piston (2), determining the opening of the alimentation valve (3) and allowing the air passage from the auxiliary reservoir to the brake cylinder. When the distributor pressure has overcome the spring pre-loading condition, the sub-assembly gets attached to the alimentation piston, determining a non-differential contribution of the distributor pressure since it acts with the same magnitude both at the top and end piston area (as shown by the red arrows in Figure 10b). In this case, the alimentation valve opening is driven by the command pressure and the load-dependent action is started. In Figure 11, the first braking phase peak detection model is shown. The first braking phase model identifies fluctuations in the distributor pressure resulting from the activation of the accelerated chamber, which temporarily reduces the distributor pressure. The model determines p_{ref} as the distributor pressure at which the accelerated chamber begins operating, defining t_{start} as the activation start time and t_{end} as the time when the chamber is fully filled, causing the distributor pressure to exceed the threshold p_{ref}. In particular, p_{ref} is not a fixed parameter in the model; it is automatically detected and varies based on the braking action initiated by the locomotive and the distance between the locomotive and the wagon.

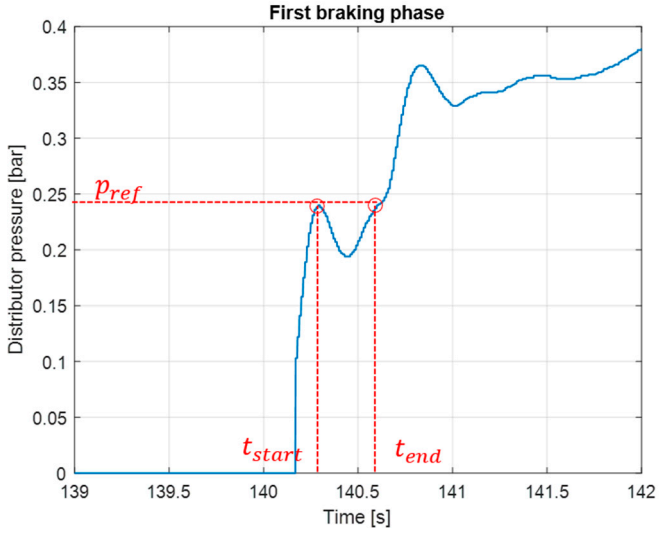

Figure 11. First braking phase peak detection.

In Figure 12, the model for the first braking phase is shown. As shown in Figure 10a, the partial reduction in distributor pressure (p_d) at a specific brake cylinder pressure causes the alimentation piston (2) and valve (3) to move downward, leading to the closure of the alimentation valve opening area. This reduction, driven by the accelerated chamber filling mechanism, results in the characteristic isobaric transformation of the brake cylinder pressure, observed as a constant value p_{bc} during the first braking phase. In case the alimentation valve is fully opened, the brake cylinder pressure derivative ($\dot{p}_{bc}$) follows the brake mode pressure variation identified as the ratio between the maximum pressure reached at the brake cylinder (identified as Pmax in Table 1) and the normative braking time, which depends on the brake mode activated (identified as Tchar in Table 1) [33,34].

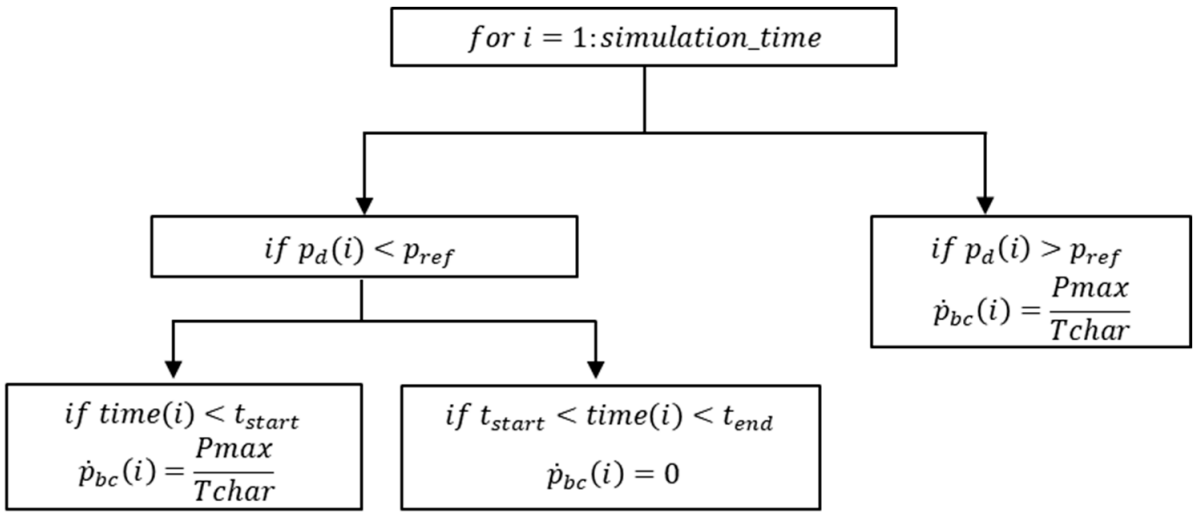

Figure 12. First braking phase model.

2.3.5. Kink Valve

The kink valve (labelled with (5) in Figure 6) is a mechanical component positioned between the distributor and brake cylinder. A simplified scheme of the kink valve is shown in Figure 13.

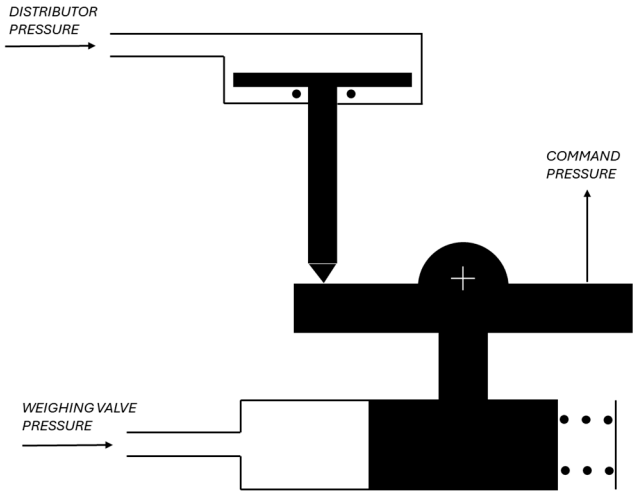

Figure 13. Simplified scheme of the kink valve.

Through a leverage mechanism, the kink valve develops a command pressure as the combination of the distributor and the weighing valve pressure (p_w). It allows for load-dependent behaviour of the brake cylinder pressure when the first braking phase has

expired. The kink valve has been modelled with the empirical transfer functions shown in Figure 14a for braking and in Figure 14b for releasing. The empirical transfer functions have been derived from the technical specifications of the kink valve provided by the component manufacturer.

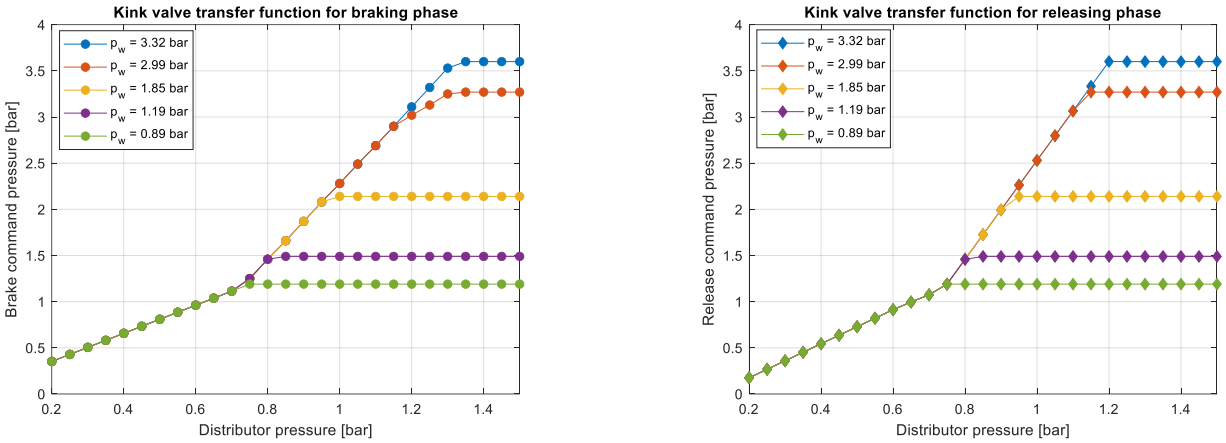

(**a**) (**b**)

Figure 14. Kink valve transfer function of (**a**) the braking phase and (**b**) the releasing phase.

These transfer functions can be divided into two parts, reflecting two different working modes of the air brake system. For distributor pressure ranging from 0.2 bar to 0.7 bar (respectively identified as K0 and K1 in Table 1), the kink valve S mode is activated. This mode is mainly used for low braking applications (service brake) when no load dependency is needed. This is done to avoid wheel blockage and slippage. For distributor pressure higher than 0.7 bar and lower than 1.36 bar for the braking phase and 1.2 bar for the releasing phase (respectively identified as LIM1 and LIM2 in Table 1), the SS mode is activated. This mode is mainly used for high braking applications (full-service brake and emergency brake) when load dependency is needed. This is done to avoid poor braking application and decrease the braking distance. Comparing Figure 14a to Figure 14b, it can be noticed that the load-dependence gradient of the transfer functions is steeper for releasing than for braking to account for mechanical component hysteresis and time delay (the reduction of the distributor pressure is faster than the release command pressure variation).

2.3.6. Relay Valve

The relay valve (labelled with (6) in Figure 6) controls the amount of air flux that passes from the auxiliary reservoir to the brake cylinder. The relay valve opening area is controlled by the pressure difference between the distributor pressure and the brake cylinder pressure during the first braking phase and by the pressure difference between the command pressure and the brake cylinder pressure during the brake build-up. In Figure 15, a simplified scheme for a relay valve is shown.

As shown in Figure 16, the pressure variation in the brake cylinder ($\dot{p}_{bc}$) is modelled as the saturation of the G | P mode device according to the variation of the alimentation valve section. This variation is derived as the pressure difference between the command pressure (p_c) and the brake cylinder pressure (p_{bc}). If the pressure difference exceeds a certain threshold (identified as EQP in Table 1), the brake cylinder pressure variation follows the G | P mode; if the pressure difference is lower than the threshold, the brake cylinder pressure variation follows the saturation of the G | P mode. The threshold has been empirically tuned to simulate the equivalent stiffening spring contribution of the relay valve components. The G | P mode has been modelled with a linear behaviour of the brake cylinder pressure with respect to the filling time, as already highlighted in Section 2.3.4. From a physical point of view, the G | P device changes the cross-sectional area connecting

the auxiliary reservoir to the brake cylinder, resulting in different filling times. The freight-passenger device was developed because freight trains are usually longer and heavier than passenger ones. Considering the delay in the propagation of braking command from the train head to its tail, freight trains are, in general, subjected to higher coupling forces, which can undermine both their safety and integrity [27]. The G brake mode allows pressure build-up to be completed within a time of around 24 s, while the P brake mode allows pressure build-up to be completed within a time of around 4 s. For long freight trains, to reduce the coupling forces difference between wagons, usually, the first five wagons after the locomotive are in G mode while the following wagons are in P mode.

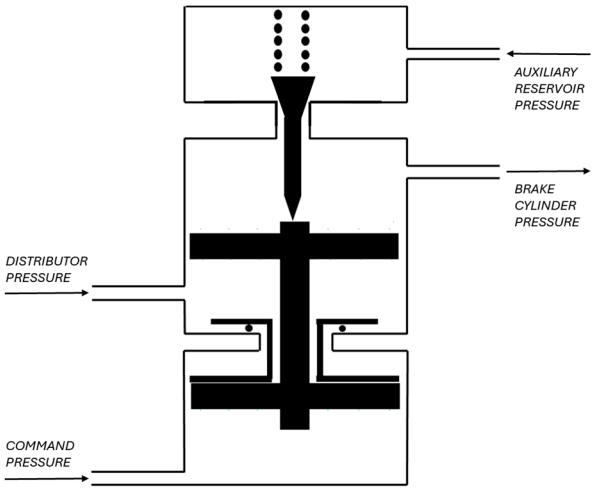

Figure 15. Simplified scheme of the relay valve.

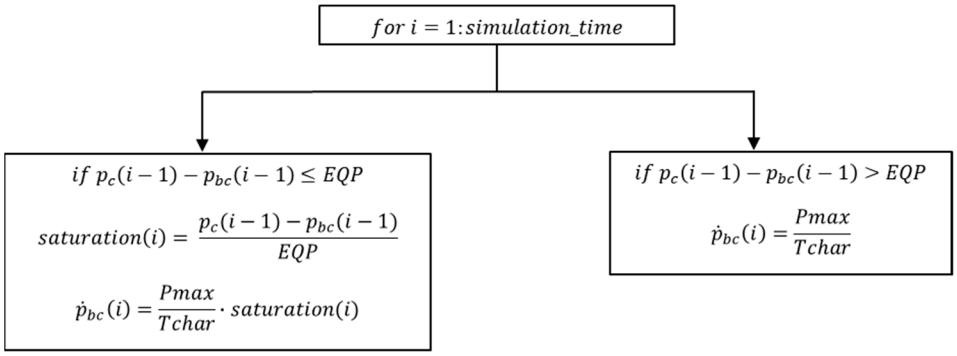

Figure 16. Alimentation valve opening model for braking phase.

2.3.7. Brake Release Valve

The release phase is modelled through the connection of the brake cylinder to the atmosphere by the brake release valve (identified with (7) in Figure 6). The release phase begins when the distributor pressure drops below the release activation threshold (identified as Sact in Table 1). This parameter has been empirically tuned to model the mechanical delay during the release process, causing the release activation time in the main brake pipe to differ from that in the brake cylinder. The orifice mass flow rate has been modelled using Equation (3) as a function of the brake cylinder pressure (p_{bc}), the brake release valve inlet temperature (identified as T_{in} in Table 1) and the atmospheric pressure (identified as p_{atm} in Table 1). While the brake cylinder pressure is iteratively calculated by the model at each simulated time, the inlet temperature is considered constant since the efflux is modelled as an isothermal transformation [35]. Additionally, atmospheric pressure is treated as a

constant physical parameter. The orifice area (identified as A in Table 1 for freight brake mode) has been experimentally estimated based on the observed releasing time.

$$\dot{m} = AC_qC_M\frac{P_{bc}}{\sqrt{T_{in}}} \tag{3}$$

where C_M is a correction factor that is calculated from an isentropic approach to the problem [36], as shown in Equation (4).

$$C_M = \begin{cases} \sqrt{\frac{2\gamma}{R(\gamma-1)}}\sqrt{\left(\frac{P_{bc}}{P_{atm}}\right)^{\frac{2}{\gamma}} - \left(\frac{P_{bc}}{P_{atm}}\right)^{\frac{(\gamma+1)}{\gamma}}}, \text{subsonic} \\ \sqrt{\frac{2\gamma}{R(\gamma-1)}}\left(\frac{2}{\gamma+1}\right)^{\frac{1}{(\gamma-1)}}, \text{supersonic} \end{cases} \tag{4}$$

Due to the irreversibility of the thermodynamic process, an empirical correction factor C_q evaluated according to the Perry correlation (proposed in [23]) is considered, as shown in Equation (5).

$$\begin{aligned} C_q = 0.8414 - 0.1002\left(\frac{P_{bc}}{P_{atm}}\right) + 0.8415\left(\frac{P_{bc}}{P_{atm}}\right)^2 - 3.9\left(\frac{P_{bc}}{P_{atm}}\right)^3 \\ + 4.6001\left(\frac{P_{bc}}{P_{atm}}\right)^4 - 1.6827\left(\frac{P_{bc}}{P_{atm}}\right)^5 \end{aligned} \tag{5}$$

The saturation of the efflux orifice area is simulated with a similar approach to the algorithm presented in Figure 16 to account for the command pressure during releasing. The cross-sectional area of the orifice can be changed to account for the P | G mode different releasing time of around 17.5 s for passengers and 52.5 s for freight [33]. Knowing the orifice mass flow rate, the continuity equation can be applied to evaluate the brake cylinder pressure at the brake release valve. This is achieved by specifying the brake cylinder volume, represented as Vmin or Vmax in Table 1, depending on whether the efflux occurs with the minimum or maximum brake cylinder volume. These parameters were obtained from the wagon's technical specification provided by Mercitalia Intermodal.

3. Results and Discussion

3.1. Experimental Model Validation

In Table 1, the model brake system parameters used for validation are shown.

The model is built on a total of 18 parameters, described in detail in Section 2.3 for each air brake component. Tchar, Dmax and Pmax are derived from the UIC 540 Standard, which provides guidelines and specifications for railway braking systems. Tin, R and patm are physical variables assumed to remain constant within the model. The remaining 12 parameters pertain specifically to the brake system modelled: some of them are obtained directly from the T3000e wagon's technical specifications, while others are empirically tuned to reflect the actual operating principles of the air brake system due to the absence of measured data for these parameters.

The dataset used for model validation was obtained from a previous field campaign, which was reported in [28]. To validate the model, the overall dataset was divided into two smaller subsets to assess the model's accuracy based on variations in two key input parameters: the braking action, which influences the main brake pipe pressure, and the wagon loading condition, which affects the weighing valve pressure. The model parameters listed in Table 1 were kept constant, as the air brake system used for validation remained unchanged. As shown in Table 2, the first model validation was carried out considering different braking actions in the main brake pipe, maintaining a constant mean pressure in the weighing valve of 2.6 bar (intermediate loading condition) and freight brake mode. In Figure 17a–c, a detailed comparison of the model and the experimental brake cylinder pressure with the input parameters described in Table 2 accounting for different braking actions is shown.

Table 2. Dataset for model validation at different braking actions.

Dataset	Brake Action	Main Brake Pipe Depression	Mean Weighing Pressure	Brake Mode
1	Service braking	0.8 bar	2.6 bar	G
2	Service braking	0.9 bar	2.6 bar	G
3	Consecutive service braking	0.74 bar	2.6 bar	G

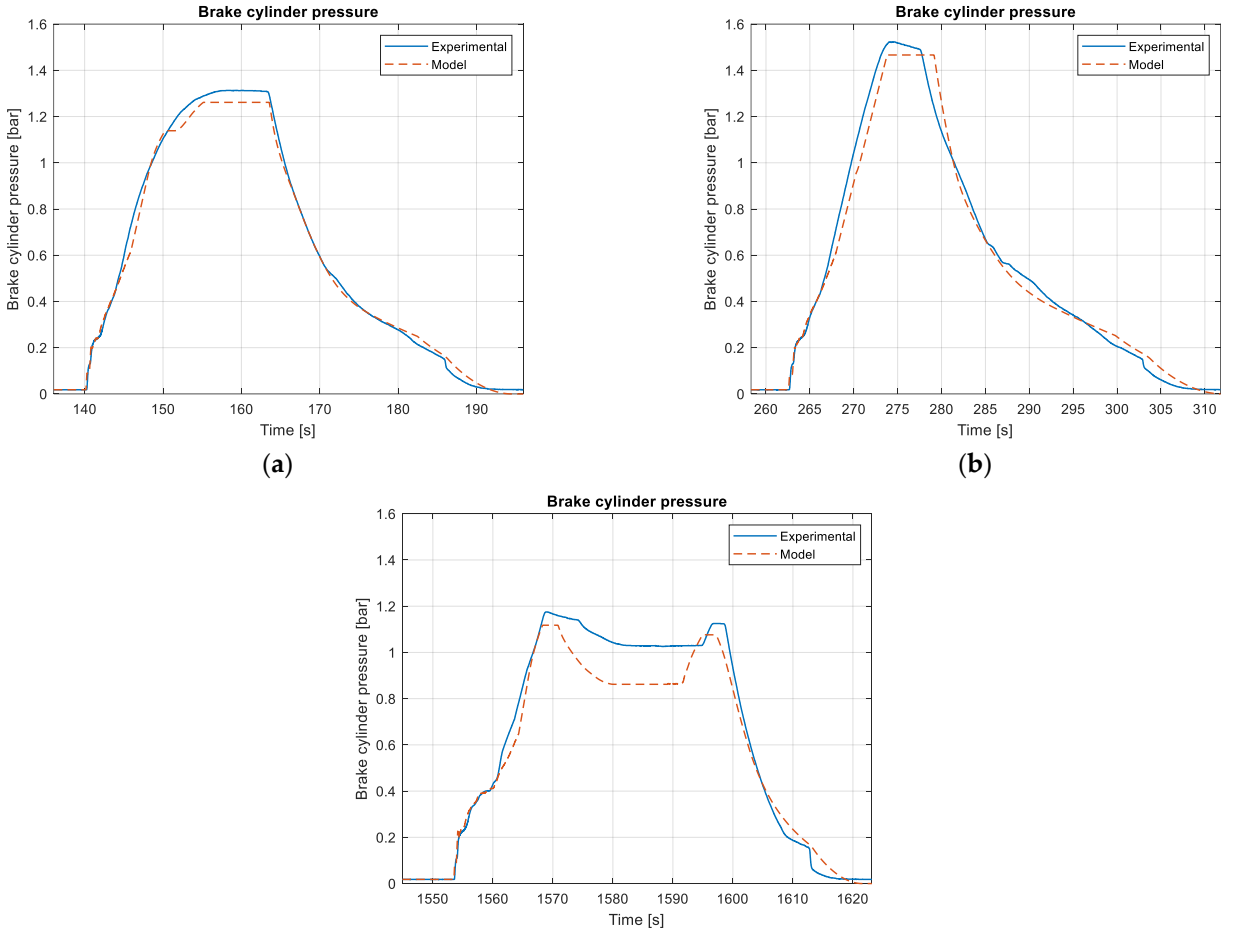

Figure 17. Comparison between the model and the experimental brake cylinder pressure with input parameters from (**a**) Dataset 1, (**b**) Dataset 2 and (**c**) Dataset 3.

As shown from the experimental comparison, the model can correctly replicate the first braking phase, the build-up phase, and the holding and the releasing phase. The main deviation comes from the incomplete release of Figure 17c, where the model underestimates the experimental pressure. The reason for this incorrect behaviour can be found in a premature activation of the realising phase from the model.

The model has also been validated on the datasets shown in Table 3, accounting for different braking actions and wagon loading conditions (Dataset 4 presents a full-loading condition, Dataset 5 presents an intermediate loading condition while Dataset 6 presents a tare loading condition). In Figure 18a–c, a detailed comparison of the model and the experimental brake cylinder pressure with the input parameters described in Table 3 accounting for different loading conditions is shown.

Table 3. Dataset for model validation at different loading conditions.

Dataset	Brake Action	Mean Weighing Pressure	Brake Mode
4	Multiple braking	3 bar	G
5	Multiple braking	2.5 bar	G
6	Emergency braking	1 bar	G

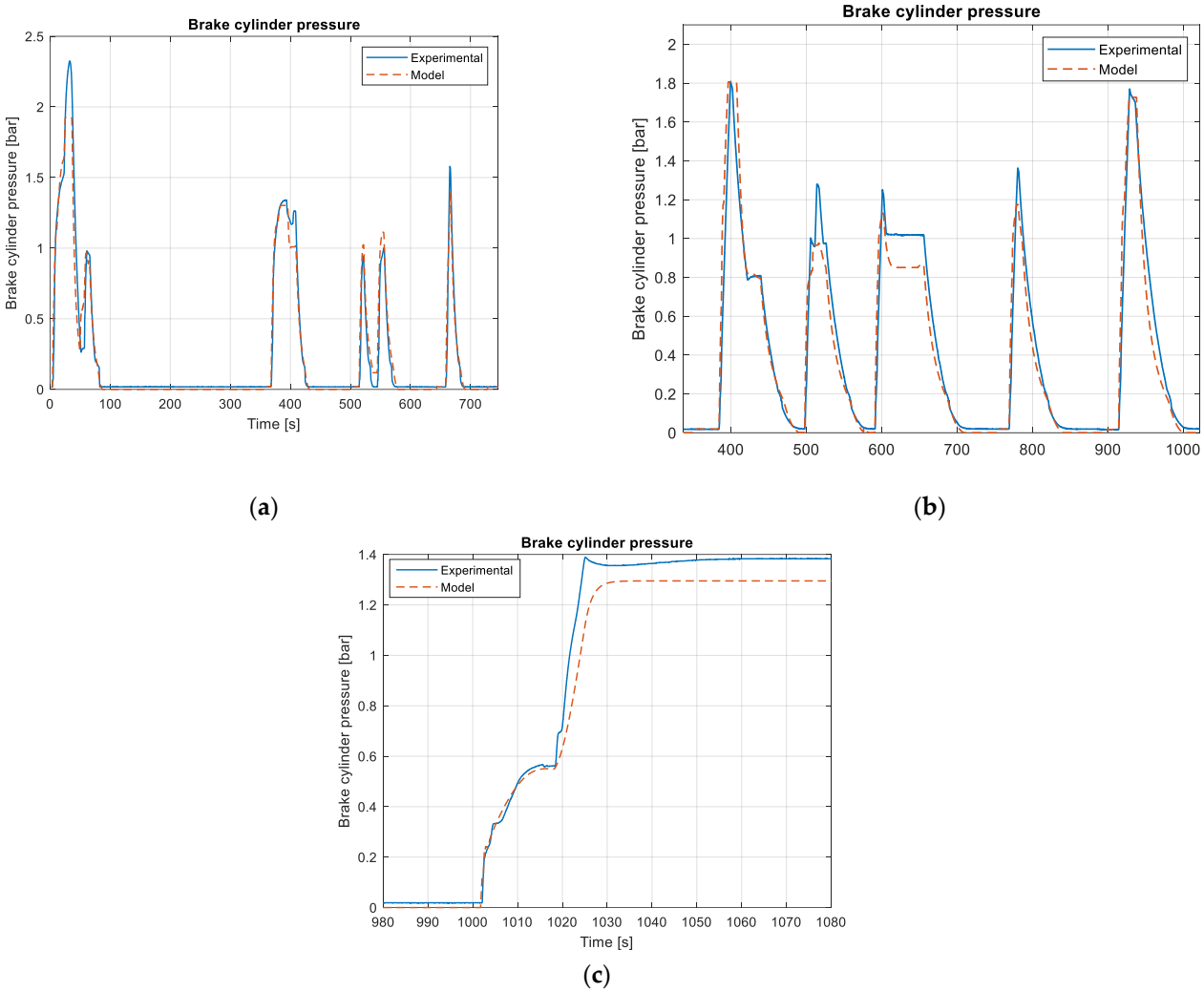

Figure 18. Comparison between the model and the experimental brake cylinder pressure with input parameters from (**a**) Dataset 4, (**b**) Dataset 5 and (**c**) Dataset 6.

Overall, the model is able to replicate correctly the brake cylinder pressure with different braking actions and wagon loading conditions. As shown in Figure 18c, the model is also able to replicate correctly emergency braking. Unfortunately, during the campaign described in [28], only datasets with freight brake mode (G) were monitored. Future experimental campaigns will provide further model validation accounting also for different brake modes.

3.2. Discussion

The relative error between the model and experimental brake cylinder pressure is used as a statistical indicator to assess the accuracy of the results, as shown in Equation (6).

$$\text{Relative error} = \frac{1}{n}\sum_{i=1}^{n}\frac{\left|p_{\text{bc model}}(i) - p_{\text{bc experimental}}(i)\right|}{\left|p_{\text{bc experimental}}(i)\right|}\cdot 100\% \quad (6)$$

The error is calculated individually for each phase to evaluate the model's performance in detail. For Datasets 4 and 5, which include multiple braking actions, the overall relative error is calculated as the average of the relative errors for each individual braking action. As illustrated in Figure 19a, the model accurately reproduces the experimental brake cylinder pressure, with a maximum relative error of 14% observed during the holding phase of Dataset 4. Figure 19b highlights the statistical variation of the relative error across phases, showing that the mean relative error remains below 10% for all phases. This demonstrates the model's reliability in simulating standard air brake operating conditions. Since the ultimate objective, as outlined in Figure 1, is to use the model for developing diagnostic algorithms, achieving high accuracy in replicating nominal air brake behaviour is a highly encouraging result. In this framework, higher variations in relative errors from the one expected may serve as indicators of potential air brake system malfunctions. Furthermore, the model exhibits good accuracy in reproducing the first braking phase, resulting in a lower mean relative error compared to other phases.

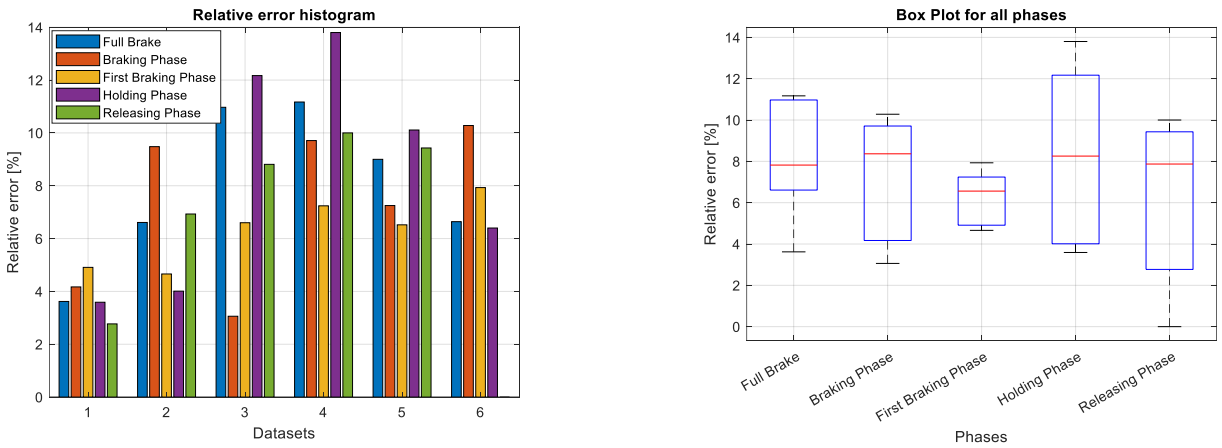

Figure 19. Relative error comparison between the model and the experimental brake cylinder pressure (**a**) for each Dataset at different phases and (**b**) for all Datasets at different phases.

To enhance the efficiency of the air brake system diagnostics, the model must accurately simulate not only the brake cylinder pressure but also the timing of each phase. While the model may effectively describe the pressure during the holding phase, it is equally important to accurately estimate the time required to reach that condition. Monitoring the timing of different phases is, in fact, crucial for malfunction identification. For instance, issues with the distributor that regulates the system's filling time could manifest as irregularities in phase timing.

To assess this aspect, the relative error in the braking phase time, defined as the time required to reach 90% of the maximum brake cylinder pressure, is calculated. A comparison is made with existing results from the literature [27], which provides a detailed analysis of braking times during emergency braking actions. As shown in Figure 20, the model demonstrates a strong correlation with results reported in [27], highlighting its reliability in capturing both pressure dynamics and phase timing.

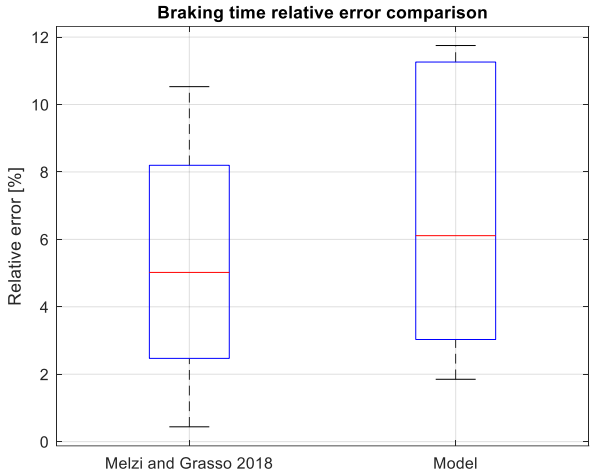

Figure 20. Comparison between the braking time calculated in [27] and the braking time coming from the model.

Although the model achieves comparable results to those in [27] when evaluating braking time, it introduces several innovative features and contributions. Notably, the air brake model in this study incorporates critical components such as the weighing valve, relay valve and kink valve, enhancing both its realism and functionality. Additionally, it accounts for the releasing phase by including the brake release valve. A major innovation is the inclusion of the first braking phase device, which captures the dynamics of the accelerated chambers. Another distinctive feature is the evaluation of brake cylinder pressure build-up as a saturation of the brake mode and the reduction of the required model parameters, optimising the computational costs. However, some limitations of the model should still be considered. Since the air brake pipe is not included in the model, the evaluation of the brake cylinder pressure can outline possible malfunctions in other brake system components without providing detailed insights into specific issues. This study validated the model based on a specific air brake system, but future work should extend its application to other air brake configurations. Additionally, most parameters are derived from the UIC European standards, limiting the model's applicability to systems governed by different standards. As noted in the previous Subsection, further validation incorporating passenger brake mode is still needed.

4. Conclusions and Future Developments

The increase in safety and reliability of freight trains can be achieved through the implementation of real-time onboard monitoring systems that are able to use models and diagnostic algorithms to identify possible malfunctions in the system. A hybrid air brake model relying on both empirical and fluid-dynamic equations has been developed in this paper for freight train air brake system monitoring. Compared to fluid-dynamic models, the low computational cost for real-time application has been achieved through the reduction of the air brake system parameters and by the feed-forward approach for estimating the brake cylinder pressure from the main brake pipe pressure. The block schematisation of the main air brake components, each with its own transfer function, enables model generalisation to wagons with different air brake systems. A new model of the first braking phase based on the correlation between the brake cylinder pressure and the distributor pressure has been developed. As shown from the experimental comparison, the model is able to correctly replicate the different braking phases of the brake cylinder at different braking actions and wagon loading configurations. The high accuracy reached by the model in replicating nominal air brake conditions makes it well-suited for the future development of model-based diagnostic algorithms. For a final and complete validation of the air brake model presented in this paper, future tests in the confined environment of the RFI San Donato test circuit have been planned to account for different braking modes.

Moreover, real-world braking defects such as leakage in the weighing valve and auxiliary reservoir will be replicated, and the air brake model will be adopted to develop a diagnostic algorithm for the detection of malfunctions in freight train air brake systems. Additionally, to better address the accuracy of the model, future validation of each component using FEM simulations could be adopted.

Author Contributions: Conceptualisation, A.G.; methodology, F.Z. and G.T.; software, A.G.; validation, A.G. and F.Z.; formal analysis, A.G.; investigation, A.G.; resources, A.G., F.Z. and G.T.; data curation, A.G. and F.Z.; writing—original draft preparation, A.G.; writing—review and editing, F.Z. and G.T.; visualisation, F.Z.; supervision, G.T.; project administration, G.T.; funding acquisition, G.T. All authors have read and agreed to the published version of the manuscript.

Funding: This study was carried out within the MOST—Sustainable Mobility National Research Centre and received funding from the European Union Next-GenerationEU (PIANO NAZIONALE DI RIPRESA E RESILIENZA (PNRR—NATIONAL RECOVERY AND RESILIENCE PLAN)—MISSIONE 4 COMPONENTE 2, INVESTIMENTO 1.4 (MISSION 4 COMPONENT 2, INVESTMENT 1.4)—D.D. 1033 17/06/2022, CN00000023). This manuscript reflects only the authors' views and opinions; neither the European Union nor the European Commission can be considered responsible for them.

Institutional Review Board Statement: Not applicable.

Informed Consent Statement: Not applicable.

Data Availability Statement: The original contributions presented in the study are included in the article, further inquiries can be directed to the corresponding author.

Acknowledgments: This work has been carried out in collaboration with Mercitalia Intermodal (Polo Mercitalia—Gruppo FS Italiane).

Conflicts of Interest: The authors declare no conflicts of interest.

References

1. Asperti, M.; Zanelli, F.; Sabbioni, E. Data-driven design of a derailment detection system for freight wagons. *Proc. Insit. Mech. Eng. Part F J. Rail Rapid Transit* **2024**, *230*, 1246–1258. [CrossRef]
2. Moya, I.; Perez, A.; Zabalegui, P.; de Miguel, G.; Losada, M.; Amengual, J.; Adin, I.; Mendizabal, J. Freight Wagon Digitalization for Condition Monitoring and Advance Operation. *Sensors* **2023**, *23*, 7448. [CrossRef] [PubMed]
3. Zanelli, F.; Sabbioni, E.; Carnevale, M.; Mauri, M.; Tarsitano, D.; Castelli-Dezza, F.; Debattisti, N. Wireless sensor nodes for freight trains condition monitoring based on geo-localized vibration measurements. *Proc. Insit. Mech. Eng. Part F J. Rail Rapid Transit* **2023**, *237*, 193–204. [CrossRef]
4. Giunta, M. Trends and Challenges in Railway Sustainability: The State of the Art regarding Measures, Strategies, and Assessment Tools. *Sustainability* **2023**, *15*, 16632. [CrossRef]
5. Ward, C.P.; Weston, P.F.; Stewart, E.J.C.; Li, H.; Goodall, R.M.; Roberts, C.; Mei, T.X.; Charles, G.; Dixon, R. Condition monitoring opportunities using vehicle-based sensors. *Proc. Insit. Mech. Eng. Part F J. Rail Rapid Transit* **2011**, *225*, 202–218. [CrossRef]
6. Bosso, N.; Gugliotta, G.; Magelli, M.; Zampieri, N. Monitoring of railway freight vehicles using onboard systems. *Procedia Struct. Integr.* **2019**, *24*, 692–705. [CrossRef]
7. Barke, D.; Chiu, W.K. Structural Health Monitoring in the Railway Industry: A Review. *Struct. Health Monit.* **2005**, *4*, 81–93. [CrossRef]
8. Li, C.; Lou, S.; Cole, C.; Spiryagin, M. An overview: Modern techniques for railway vehicle on-board health monitoring systems. *Veh. Syst. Dyn.* **2017**, *55*, 1045–1070. [CrossRef]
9. Bernal, E.; Spiryagin, M.; Cole, C. Onboard Condition Monitoring Sensors, Systems and Techniques for Freight Railway Vehicles: A Review. *IEEE Sens. J.* **2019**, *19*, 4–24. [CrossRef]
10. Cii, S.; Tomasini, G.; Bacci, M.L.; Tarsitano, D. Solar Wireless Sensor Nodes for Condition Monitoring of Freight Trains. *IEEE Trans. Intell. Transp. Syst.* **2020**, *23*, 3995–4007. [CrossRef]
11. Gruden, M.; Hinnemo, M.; Dancila, D.; Zherdev, F.; Edvinsson, N.; Brunberg, K.; Andersson, L.; Bystrom, R.; Rydberg, A. Field operational testing for safety improvement of freight trains using wireless monitoring by sensor network. *IET Wirel. Sens. Syst.* **2014**, *4*, 56–60. [CrossRef]
12. Macucci, M.; Di Pascoli, S.; Marconcini, P.; Tellini, B. Wireless sensor network for derailment detection in freight trains powered from vibrations. In Proceedings of the 2015 IEEE International Workshop on Measurements and Networking, Coimbra, Portugal, 12–13 October 2015.
13. Shi, D.; Ye, Y.; Gillward, M.; Hecht, M. Robustness enhancement of machine fault diagnostic models for railway applications through data augmentation. *Mech. Syst. Signal Process.* **2022**, *164*, 108217. [CrossRef]

14. Kulkarni, R.; Carlsonn, U.; Qazizadeh, A.; Stichel, S. Vehicle running instability detection algorithm (VRIDA): A signal based onboard diagnostic method for detecting hunting instability of rail vehicles. *Proc. Insit. Mech. Eng. Part F J. Rail Rapid Transit* **2022**, *236*, 262–274. [CrossRef]
15. GB Railfreight Successfully Trials Innovative Brake Monitoring IoT System. Available online: https://www.icomera.com/gb-railfreight-successfully-trials-innovative-brake-monitoring-iot-system/#_ftn2 (accessed on 23 October 2024).
16. Fresh Essays. Railway Brake Systems Failure. Available online: https://samples.freshessays.com/railway-brake-systems-failure.html (accessed on 17 June 2024).
17. Rail Accident Report. Runaway and Derailment of Wagons at Ashburys, 4 May 2010. Available online: https://www.gov.uk/raib-reports/runaway-and-derailment-of-wagons-at-ashburys (accessed on 28 November 2024).
18. European Commission. *Development of the Future Rail Freight System to Reduce the Occurrences and Impact of Derailment*; D1.1 Summary Report and Database of Derailments Incidents; European Commission: Brussels, Belgium, 2024.
19. Kasimov, O.T.; Mamaev, S.I.; Grishenko, A.V. Causes of rolling stock brake equipment failure. *Tech. Sci. Innov.* **2021**, *2021*, 302–306.
20. Hou, Z.; Lee, C.K.M.; Lv, Y.; Keung, K.L. Fault detection and diagnosis of air brake system: A systematic review. *J. Manuf. Syst.* **2023**, *71*, 34–58. [CrossRef]
21. Pfaff, R.; Enning, M.; Sutter, S. A risk-based approach to automatic brake tests for rail freight service: Incident analysis and realisation concept. *SN Appl. Sci.* **2022**, *4*, 115. [CrossRef]
22. Wu, Q.; Cole, C.; Spiryagin, M.; Chang, C.; Wei, W.; Ursulyak, L.; Shvets, A.; Murtaza, M.A.; Mirza, I.M.; Zhelieznov, K.; et al. Freight train air brake models. *Int. J. Rail Transp.* **2021**, *11*, 1–49. [CrossRef]
23. Ge, X.; Chen, Q.; Ling, L.; Zhai, W.; Wang, K. An approach for simulating the air brake system of long freight trains based on fluid dynamics. *Railw. Eng. Sci.* **2023**, *31*, 122–134. [CrossRef]
24. Wu, Q.; Cole, C.; Spiryagin, M.; Wang, Y.; Ma, W.; Wei, C. Railway Air Brake Model and Parallel Computing Scheme. *J. Comput. Nonlinear Dyn.* **2017**, *12*, 051017. [CrossRef]
25. Bosso, N.; Magelli, M.; Zampieri, N. A numerical method for the simulation of freight train emergency braking operation based on the UIC braked weight percentage. *Railw. Eng. Sci.* **2023**, *31*, 162–171. [CrossRef]
26. Martin, G.C.; Hay, W.W. *Method of Analysis for Determining the Coupler Forces and Longitudinal Motion of a Long Freight Train*; University of Illinois: Urbana, IL, USA, 1967.
27. Melzi, S.; Grasso, A. Development of a numerical model of railway air brake and validation against experimental data. *J. Adv. Veh. Eng.* **2018**, *5*, 10–17.
28. Zanelli, F.; Mauri, M.; Castelli Dezza, F.; Sabbioni, E.; Tarsitano, D.; Debattisti, N. Energy Autonomous Wireless Sensor Nodes for Freight Train Braking System Monitoring. *Sensors* **2022**, *22*, 1876. [CrossRef] [PubMed]
29. Zanelli, F.; Galimberti, A.; Debattisti, N.; Mauri, M.; Tarsitano, D.; Osorio Mendoza, C.; Negri, S.; Tomasini, G. Design of a Modular and Integrated On-Board System for Freight Train Condition Monitoring. In Proceedings of the Sixth International Conference on Railway Technology: Research, Development and Maintenance, Prague, Czech Republic, 1–5 September 2024.
30. Galimberti, A.; Zanelli, F.; Debattisti, N.; Negri, S.; Castelli Dezza, F.; Tomasini, G. Energy harvesting for freight train monitoring system. In Proceedings of the IEEE International Conference on Environment and Electrical Engineering, Rome, Italy, 17–20 June 2024.
31. Matlab R2021b. Available online: https://it.mathworks.com/products/matlab.html (accessed on 2 April 2024).
32. Description and Technical Specification of the Double Articulated Pocket Wagon Type T3000e. Available online: https://www.txlogistik.eu/wp-content/uploads/T3000e_technical_specification_30.pdf (accessed on 5 April 2024).
33. *UIC 540*; Freins a Air Comprimè pour Trains de Merchandises et Trains de Voyageurs. International Union of Railways (UIC): Paris, France, 2016.
34. Crescentini, E. Sviluppo di un Codice di Simulazione Dinamica per lo Studio di Treni Merci di Futura Generazione. Ph.D. Thesis, Tor Vergata, Roma, Italy, 2008.
35. Pugi, L.; Malvezzi, M.; Allotta, B.; Banchi, L.; Presciani, P. A parametric library for the simulation of a Union Internationale des Chemis de Fer (UIC) pneumatic braking system. *Proc. Insit. Mech. Eng. Part F J. Rail Rapid Transit* **2003**, *218*, 117–132. [CrossRef]
36. *ISO 6538:1989*; Pneumatic Fluid Power—Components Using Compressible Fluids—Determination of Flow Rate Characteristics. Internation Standardization Organization: Geneva, Switzerland, 21 September 1989.